Available online at www.sciencedirect.com
SCIENCE DIRECT®
Ocean Modelling 11 (2006) 464–477
Ocean Modelling
www.elsevier.com/locate/ocemod

Barotropic tidal mixing effects in a coupled climate model: Oceanic conditions in the Northern Atlantic

Hyun-Chul Lee [a,b,*,1], Anthony Rosati [b], Michael J. Spelman [b]

[a] *RSIS, McLean, VA, USA*
[b] *NOAA, Geophysical Fluid Dynamics Laboratory, Princeton, NJ, USA*

Received 6 January 2005; received in revised form 15 March 2005; accepted 15 March 2005
Available online 11 May 2005

Abstract

Impacts of mixing driven by barotropic tides in a coupled climate model are investigated by using an atmosphere–ocean–ice–land coupled climate model, the GFDL CM2.0. We focus on oceanic conditions of the Northern Atlantic. Barotropic tidal mixing effects increase the surface salinity and density in the Northern Atlantic and decrease the RMS error of the model surface salinity and temperature fields related to the observational data.

1. Introduction

It is known that 70–80% of total tidal energy is dissipated by the bottom friction of the barotropic tidal motion in shallow marginal seas, and there is currently debate over the importance of the mixing (Munk and Wunsch, 1998; St. Laurent et al., 2002). Many numerical studies of coastal regions have considered realistic and integrated tidal mixing for the coastal process (Lynch et al., 1996; Holloway, 2001; Werner et al., 2003). Because of its short time scale and the small spatial scale of shallow coastal regions, however, the barotropic tide traditionally has been excluded from

* Corresponding author. Tel.: +1 609 987 5072.
E-mail address: hyun-chul.lee@noaa.gov (H.-C. Lee).
[1] Presently at GFDL/NOAA.

1463-5003/$ - see front matter © 2005 Elsevier Ltd. All rights reserved.
doi:10.1016/j.ocemod.2005.03.003

global climate models. Recently the effects of mixing generated by the ocean tide over rough topography have been evaluated in ocean general circulation models and open oceans (Simmons et al., 2004; Schiller, 2004; St. Laurent et al., 2002; Egbert and Ray, 2001; Jayne and St. Laurent, 2001; Nakamura and Awaji, 2004).

Barotropic tidal energy is concentrated in coastal regions with energy larger by several orders of magnitude than in deep open regions (Fig. 1). The dissipation of tidal energy induces vertical mixing in the coastal region and continental slope (Lien and Gregg, 2001; Mourn et al., 2002). This tidal mixing is important in stirring river plumes, a shelf process not resolved in our model. Our focus is on the oceanic conditions of the Northern Atlantic, which is important in the overturning

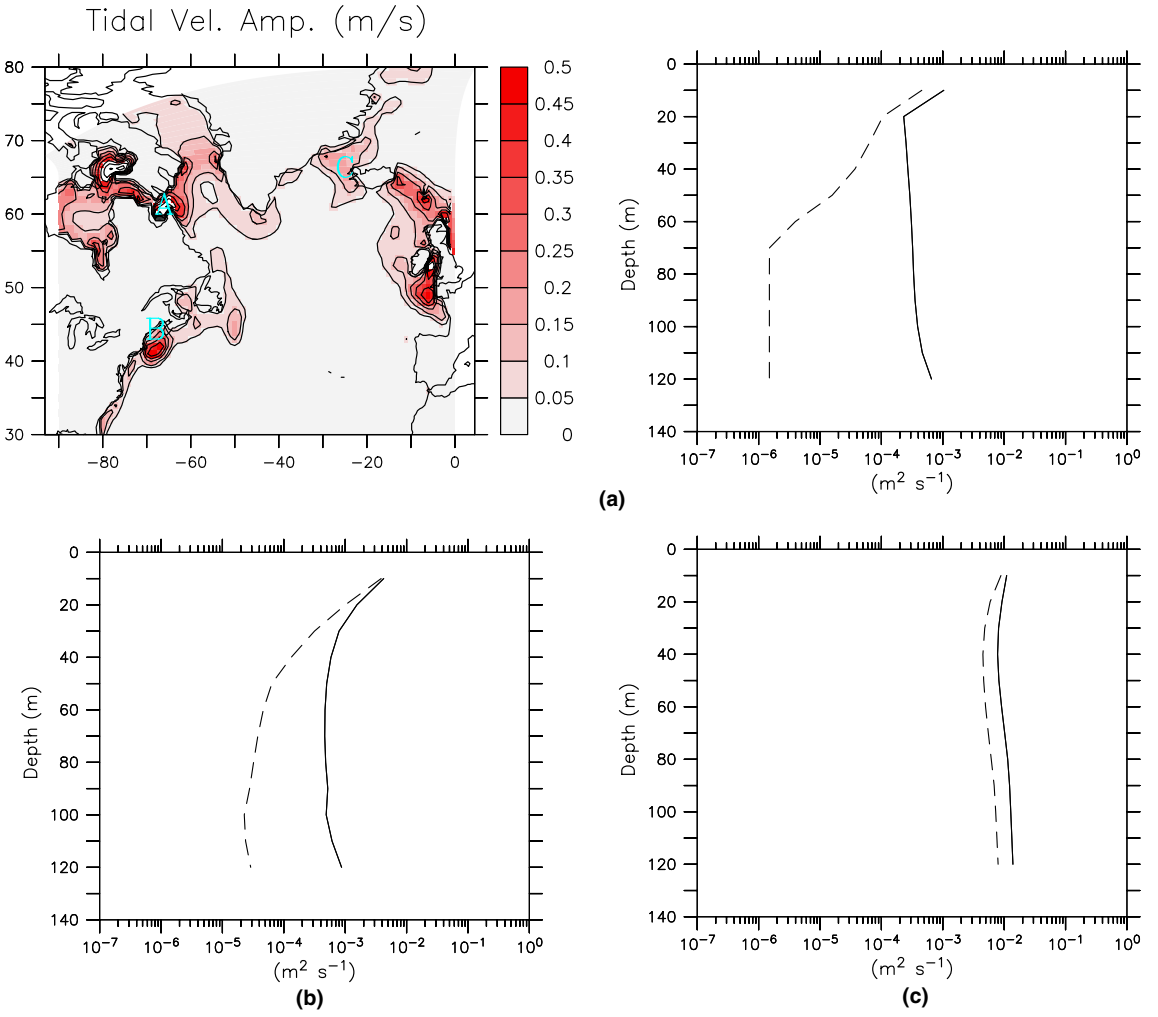

Fig. 1. Left-top panel is horizontal distribution of the tidal velocity amplitude of $M2$ component from satellite data (Egbert et al., 1994). The three profiles are vertical eddy diffusivity distribution at the three points, (a) (66° W, 60° N), (b) (68° W, 43° N), and (c) (25° W, 65° N) in the left-top panel. Solid line is the diffusivity in the case *with* tidal mixing and dashed line is *without* tidal mixing.

circulation and in which there is a systematic model bias in the sea surface salinity and temperature fields. The model bias is caused by fresh water fluxes from river discharges and ice melting, which produces low surface salinity in coastal region that is advected across the north Atlantic and inhibits the mixing due to convection. Given these facts, we try to answer the following question: Is it possible that the barotropic tidal mixing affects the sea surface conditions of the Northern Atlantic, in a coupled GCM?

In this study, the impact of tidal mixing on oceanic conditions in the Northern Atlantic has been investigated using the Geophysical Fluid Dynamics Laboratory (GFDL) coupled climate model, a developmental version of CM2.0 (Delworth et al., in press). The vertical mixing driven by barotropic tide is simply parameterized by estimating tidally driven turbulence from the observed tidal velocity amplitude. This paper is organized as follows: In Section 2, the model and experiment configurations are described. Results for the sea surface conditions in the Northern Atlantic are provided in Section 3. Summary and conclusion for tidal impacts are given in Section 4.

2. Model

2.1. Configurations

The coupled climate model used here is based on the Flexible Modeling System (FMS) of the GFDL. The new GFDL FMS is a model infrastructure for constructing and executing atmospheric, oceanic and climate system models, and allows various combinations of coupled model components: atmosphere (AM2), ocean (MOM4), land (LM2) and sea ice (SIS). GFDL GAMDT (submitted for publication) presents configurations and performance of AM2 and LM2. Griffies et al. (2003) provide computational, numerical and physical characteristics of MOM4. Winton (2000, 2003) present the formulation of the sea ice model (SIS) and its application to the coupled climate model. Here, we briefly describe each model configuration based on previous documentations.

The ocean component of the coupled model is constructed from the GFDL MOM4 code (Griffies et al., 2003). The model resolution is one degree in longitude, and changes in latitude from 0.34° near the equator to 1.0° south of 30° S and near 65° N. North of 65° N, the model grid is defined by the tripolar grid system of Murray (1996). The vertical resolution is 50 depth levels where the top 22 levels are evenly spaced in the top 220 m depth. In the ocean model, the free surface is explicitly calculated. Neutral tracer diffusion is implemented according to Griffies et al. (1998). Vertical mixing is parameterized by the KPP scheme of Large et al. (1994), which has been developed for use in global climate modeling, as are these experiments. For the bottom boundary layer, Beckmann and Döscher's scheme is embedded in the ocean model, MOM4 (Beckmann and Döscher, 1997).

The grid system of the AM2 dynamical core is the Arakawa B-grid (GAMDT, submitted for publication) with horizontal resolution of 2.5° longitude by 2.0° latitude. The atmospheric model has 24 levels in the vertical using a hybrid coordinate system.

The ice model component (SIS) is based on the ice dynamical model by Hunke and Dukowicz (1997). The thermodynamics of the SIS is defined by two ice layers and one snow layer with five ice thickness categories (Semtner, 1976; Winton, 2000).

The land model (LM2) is based on the Land Dynamics Model of Milly and Shmakin (2002). There are 18 soil layers for heat calculation. For water mass balance, soil water and ground water are not allowed to freeze. Model parameters vary spatially as functions of vegetation and soil types but are temporally invariant.

2.2. Vertical tidal mixing

Tidal motions are driven by astronomic forcing and mainly damped by bottom friction. The frictional velocity shear in the bottom boundary layer, which is induced by tidal motions, generates the vertical mixing of water mass (Simpson and Hunter, 1974). The tidal motion has a relatively short time scale and fast phase speed in comparison with those scales of phenomena in climate models. In this study, instead of resolving explicit tidal motion, the vertical mixing driven by the tide is parameterized by the vertical mixing coefficient of the ocean model, dependent on the Richardson number (Munk and Anderson, 1948; Pacanowski and Philander, 1981). The vertical diffusivity (K_z) of the tide was parameterized by the Munk–Anderson scheme, as follows

$$K_z = K_0(1 + \sigma Ri)^{-p} + K_b, \tag{1}$$

where K_0 is the maximum diffusivity due to the shear instability given by 5.0×10^{-3} m^2 s^{-1}, K_b is the background diffusivity, Ri is the Richardson number, and σ and p are coefficients given by 3.0 and 0.25, respectively. In the Richardson number,

$$Ri = \frac{N^2}{(\partial U/\partial z)^2}, \tag{2}$$

N is the Brunt–Vaisala frequency, and following the empirical logarithmic profile of current in the bottom boundary layer (James, 1977). The turbulent mixing driven by the barotropic tide occurs mainly in the bottom boundary layer, because the bottom friction induces the vertical velocity shear in the bottom boundary layer. The frictional turbulence component could be defined as

$$\left(\frac{\partial U}{\partial z}\right)^2 = 0.5\left(\frac{A}{H - z}\right)^2 \tag{3}$$

where $A = Cd^{\frac{1}{2}}V_t/k$, k is the von Karman constant (0.41), and Cd is the bottom drag coefficient (2.4×10^{-3}). V_t, is the $M2$ tidal velocity amplitude (Fig. 1) from satellite data from Egbert et al. (1994), which is static in time. The frictional velocity shear in Eq. (3) also is constant with time, but K_z is changing due to the variation of stratification.

This parameterization for the barotropic tidal mixing is applied to the whole global model basin, and the vertical diffusivity obtained from the tidal frictional turbulence is combined with the vertical diffusivity of the KPP scheme. Fig. 1 shows depth profiles of vertical diffusivity *with* (solid line) and *without* (dashed line) tidal mixing effect. In the lower layer, the tidal mixing effect increases the vertical diffusivity by three orders of magnitude at the northern shelf of Labrador Sea (location A in Fig. 1). This region of large tidal amplitude is also one where there is a large discharge of summer time river runoff. Without the increased vertical mixing the freshwater runoff would stay at the surface.

The vertical tidal mixing changes the density structure by vertical mixing, therefore the current structure is also affected by the tidal mixing in the coastal region. Detail coastal processes are not

possible to resolve in this global model, however the simple parameterization described above became necessary to represent physical processes that are included in land and ice components, i.e. river discharge and ice melting. The Munk–Anderson mixing scheme is relatively simple and not constrained by the energy budget, and we are planning to improve this simple mixing scheme into a more realistic one in the future.

3. Effects of vertical tidal mixing

In order to investigate the tidal mixing impact on a coupled climate model, two coupled experiments were carried out: control run *without* tidal mixing effect and experimental run *with* tidal mixing effect. Both experiments were executed for 100 years, and model results of the last fifty years were analyzed.

3.1. Sea surface salinity (SSS) and sea surface temperature (SST)

The vertical mixing driven by the tide directly changes salinity profiles of the coastal water mass along the western coast of the Labrador Sea. In the Labrador Sea, the surface water maintains relatively low SSS due to fresh water fluxes from the sea ice and river discharge (Fig. 2(a)). The SSS in the Labrador and the Norwegian Sea is lower than 33 PSU in the model, and there is a strong salinity gradient between the low salinity surface water of these seas and the high SSS water from the subtropical gyre in the Atlantic. The fresher water fluxes increase the hydrostatic stability in the surface layer, which inhibits convective mixing. In our coupled climate models, the fresh water fluxes from rivers and sea ice melting make the surface water in the Northern Atlantic fresher and cooler than observational data.

The tidal mixing plays an important role in homogenizing the vertical salinity profile and increasing the surface salinity fields in the Labrador Sea by mixing with lower layer water of relatively high salinity. Fig. 2(b) shows the change of the SSS field induced by the vertical tidal mixing. The vertical mixing driven by the tide increases the SSS more than 0.6 PSU along the western coastal region in the Labrador Sea and 0.4 PSU west of Iceland. Fig. 1 shows high tidal energy in Hudson Bay and suggests that the origin of the high SSS anomaly of the tide in the Labrador Sea is in the northern region, especially in the Hudson Strait. The high SSS anomaly from the tide is advected to the south along the Canadian coast and extends to the Middle Atlantic Bight. The southward movement of the coastal water is consistent with observational features of the region (Chapman and Beardsley, 1989).

It is noted that the large SSS anomaly extends from the coastal region to the open ocean. This extension of the SSS anomaly is mainly by the advection of the Gulf Stream. Lillibridge et al. (1990) referred to the entrainment and mixing of coastal water in the Gulf Stream as, so-called, Ford Water. The observed scale of Ford Water intrusion is smaller than the model resolution of CM2, however, the model consistently reproduced the general features of the intrusion and mixing of the coastal waters in the Gulf Stream.

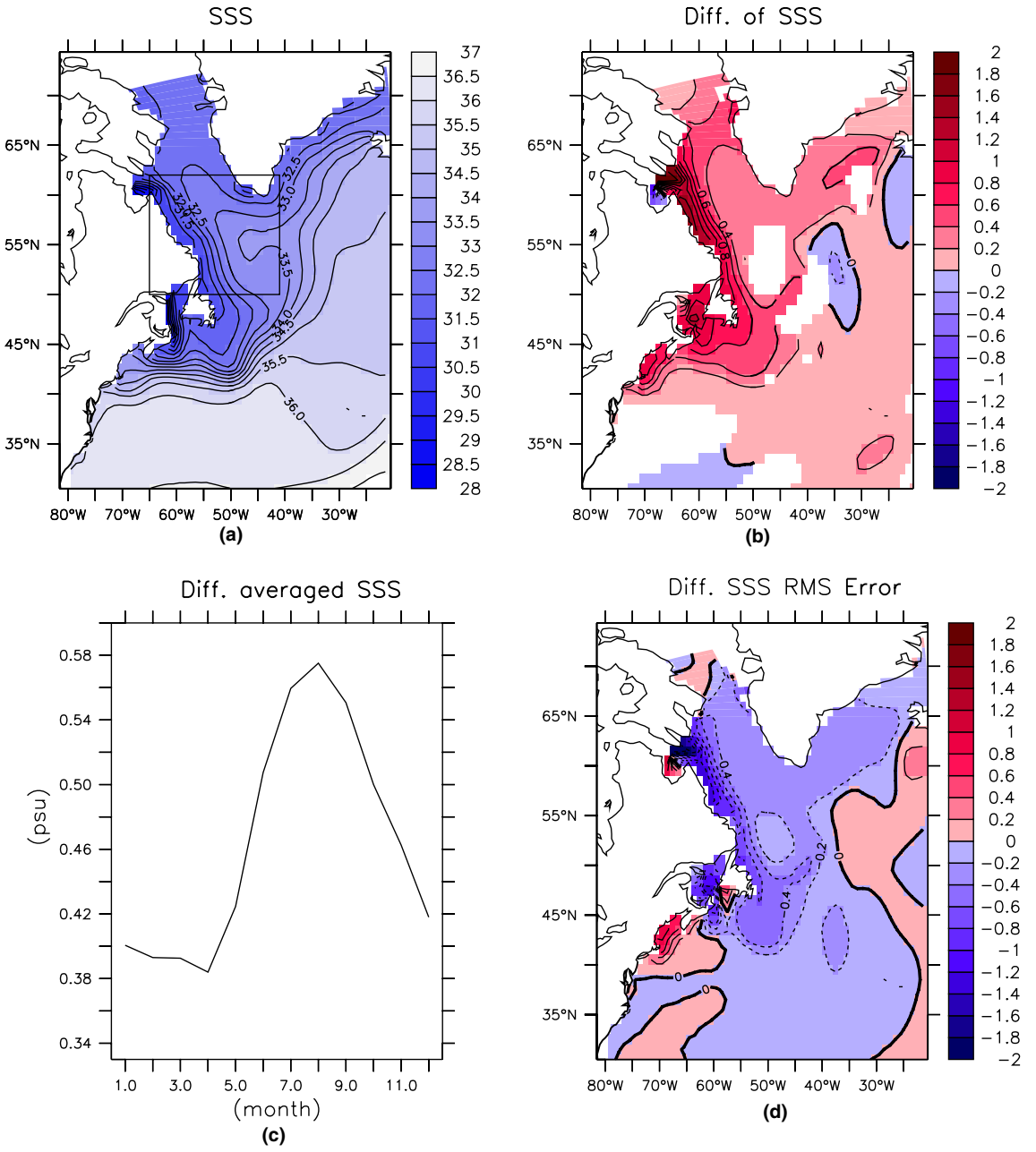

Fig. 2. (a) Fifty year averaged sea surface salinity (SSS) *with* tidal mixing. (b) Difference of SSS obtained by the subtraction of SSS *without* tidal mixing from *with* tidal mixing, masked by 95% of significance with the 300 year mean data of *with* tidal mixing. (c) Seasonal variation of the area-averaged (rectangular region in (a): 65° W–41° W, 50° N–62° N) SSS difference between *with* and *without* tidal mixing. (d) Difference of SSS RMS error for the monthly climatology of Levitus data between *with* and *without* tidal mixing.

Fig. 2(c) shows the seasonal change of the SSS difference of the vertical tidal mixing in the Labrador Sea (65° W–41° W, 50° N–62° N). The effect of the vertical tidal mixing on the SSS in Labrador Sea has seasonal variation. The maximum effect occurs in summer when fresh water fluxes from river discharge and ice melting into the ocean increases and the vertical salinity gradient increases along the coastal region. The vertical mixing of the tide decreases the SSS over the Labrador Sea by 0.58 PSU in summer and 0.4 PSU in winter.

The vertical mixing driven by the tide significantly improves the SSS field of the model. Fig. 2(d) shows the difference of SSS RMS error for the monthly climatology of Levitus data between *with* and *without* tidal mixing effect, which is obtained by subtracting the RMS error *without* tidal mixing effect for the Levitus monthly climatology, from the RMS error *with* tidal mixing effect for the Levitus monthly climatology. The minus value of the RMS difference means the model *with* tidal mixing decreases the RMS error for the monthly Levitus climatology. It is clearly seen that the SSS RMS error *with* tidal mixing effect is smaller than *without* mixing effect in the Northern Atlantic, particularly along the coastal region. The SSS RMS error *with* tidal mixing is less than 2 PSU in the Labrador Sea. The improvement due to the tidal mixing is 0.2 PSU in the central and eastern Labrador Sea, and more than 1.2 PSU in the western coast of the Labrador Sea.

The annual mean SST over the Labrador Sea and the Norwegian/Greenland Sea is below 2 °C. A strong temperature gradient of low SST water is formed with the Gulf Stream and its extension water. The distribution of this temperature front generally coincides with SSS (Fig. 3(a)).

Similar to the salinity profile, the tidal mixing vertically homogenizes the coastal water and forms relatively cold surface water. This cold SST perturbation core induced by the tidal mixing is limited to a narrow region along the western coast of the Labrador Sea (Fig. 3(b)). One noticeable difference in SST is the warm SST region southwest of Iceland. This warmer SST difference looks stable and robust, and also appears in 75-year-average and 95-year-average results. In Fig. 3(b), a series of relatively large difference of SST occurs along the northern edge of the Gulf Stream and its extension region (Fig. 3(a)). This might be due to the frontal structure and moving of the Gulf Stream axis.

Fig. 3(c) shows the annual variation of the difference of SST over the Labrador Sea (65° W–41° W, 50° N–62° N). The tidal mixing effect on the SST in the Labrador Sea is maximum in May and June (0.4 °C) and minimum in September.

The vertical mixing driven by the tide makes the surface water in the Northern Atlantic warmer, and this effect generally improves the model results in the SST field. The SST RMS error decreases in the northern North Atlantic by the tidal mixing effect.

The comparison of model results shows that the tidal mixing effect extends from the coastal region of the Labrador Sea to the middle Atlantic and makes the surface water of the Northern Atlantic more saline and warmer. The impact of the tidal mixing reduces the model bias for the surface water related to fresh water fluxes.

3.2. Sea surface density (SSD)

Due to the coldness of the surface water, the relatively high-density water more than $26.6\sigma_t$ outcrops in the northeastern Atlantic and the Labrador Sea (Fig. 4). The costal region of the Labrador Sea is strongly affected by the fresh water fluxes from rivers and ice, and SSD in the coastal region is lower than in the northeastern Atlantic (Fig. 2).

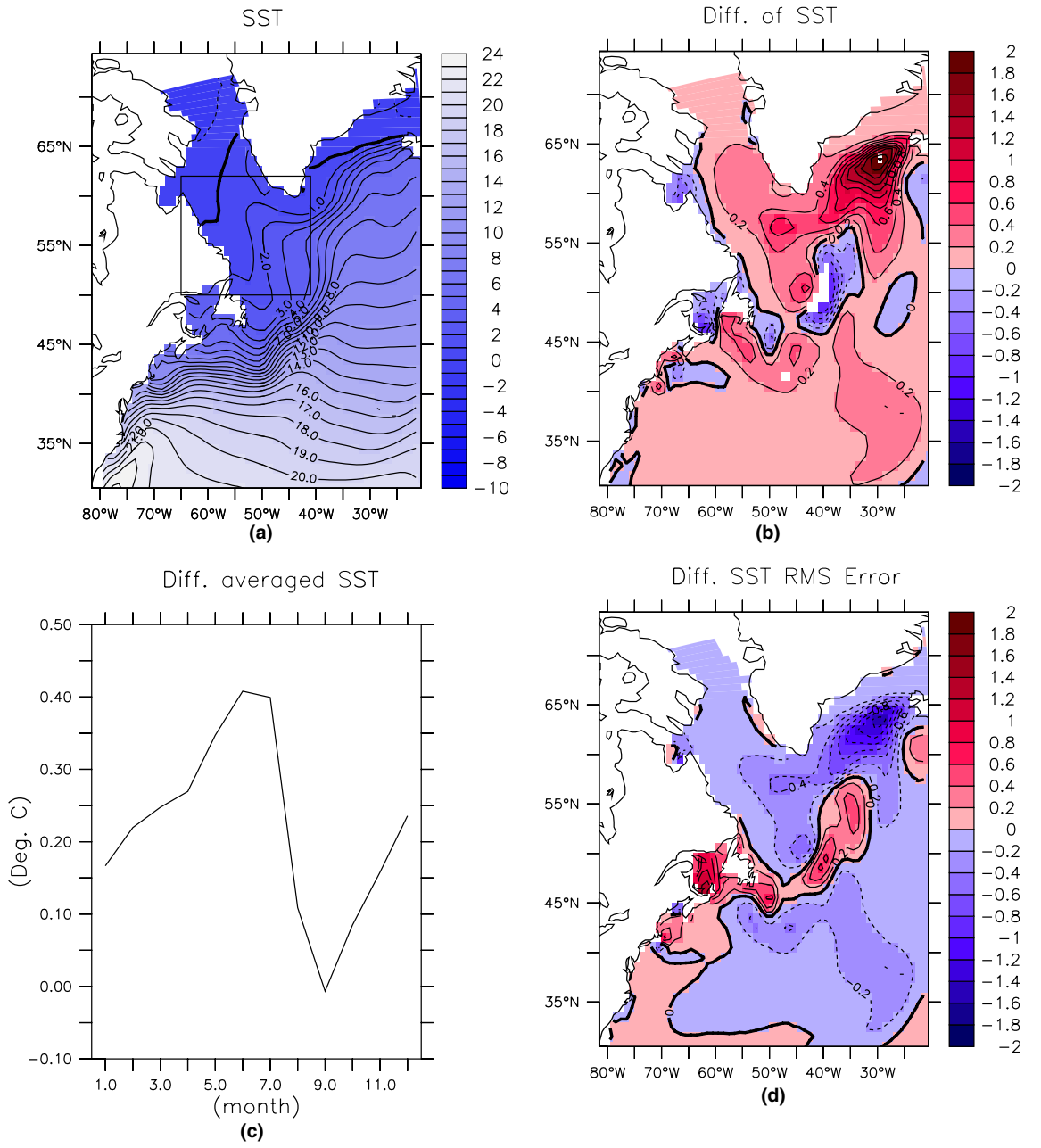

Fig. 3. Same as in Fig. 2 except for sea surface temperature.

The SSD along the western coastal region of the Middle Atlantic Bight and over the Labrador Sea increases by increasing SSS due to the tidal vertical mixing effect (Fig. 4). The difference between SSD *with* and *without* tidal mixing has similar pattern to the SSS difference (Fig. 2) as would be expected since density variations in this region are dominated by salinity variation. In the

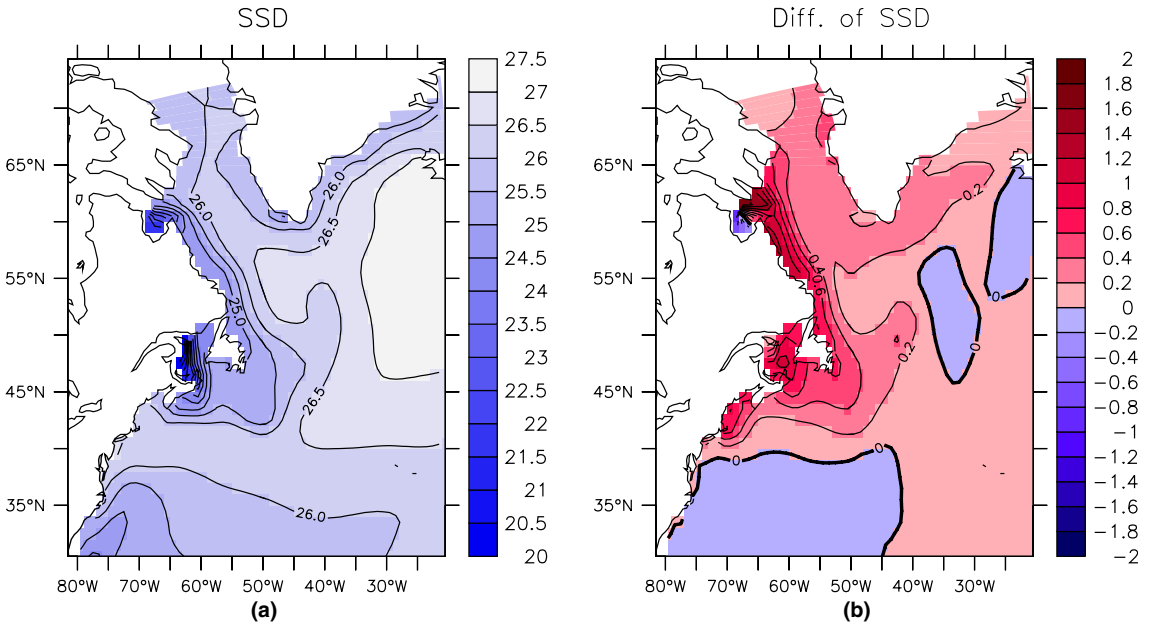

Fig. 4. Left panel is 50 year averaged sea surface density (σ_t) distribution of *with* tidal mixing. Right panel is the difference of sea surface density, which is the result *without* tidal mixing subtracted from the result *with* tidal mixing. CI is 0.2 kg/m^3.

Labrador Sea, the SSD from the experiment *with* tidal mixing is higher than *without* tidal mixing by 0.2 kg/m^3. This could impact ventilation and formation of North Atlantic Deep Water in the Labrador Sea and the meridional overturning circulation in the Atlantic.

Fig. 5 shows the vertical section of the potential density along 47.5° W. Isopycnal surfaces have the upper most of the dome-shape structure at 54° N, and the isopycnal of 26.8σ_t outcrops in the Labrador Sea. Between 52° N and 57° N, the isopycnal surface of 27.4σ_t, rises up to 150 m depth and the surface of 27.0σ_t, lies in the surface layer upper 100 m depth. Through the outcropping window, the deep water could refresh the water properties.

The difference of the potential density *with* and *without* tidal mixing effect (Fig. 5(b)) shows that the tidal mixing effect increases the water density of the Labrador Sea and is concentrated in the upper 100 m depth. In the outcropping region between 52° N and 57° N, the tidal mixing effect of increasing SSD can intensify the ventilation process and the overturning circulation of the Northern Atlantic.

3.3. Ventilation

Fig. 6 shows the sectional distribution of the water age, which represents the elapsed time since the water has been ventilated from the sea surface. Above 200 m depth, the water age is less than 5 years, where the vertical mixing process dominates. It is noticeable that below 300 m depth the water age distribution is almost vertically homogeneous. The water age becomes less at higher latitudes, which shows that the deep water formation process is active in this region. From

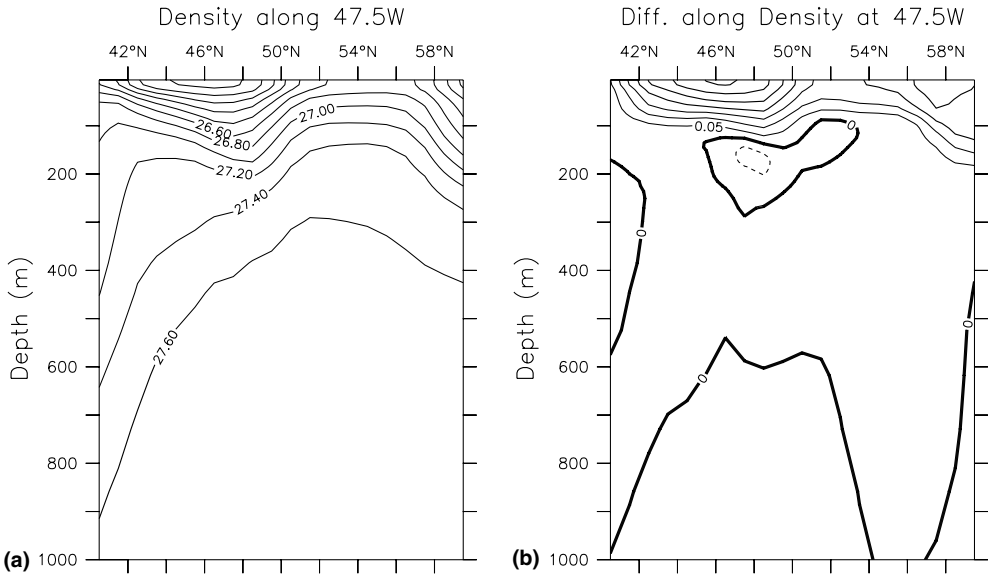

Fig. 5. (a) Fifty year averaged vertical distribution of potential density *with* tidal mixing along 47.5° W. (b) Difference of potential density along the same section, obtained by the subtraction the result *without* tidal mixing from *with* tidal mixing. Dashed lines in right panel are minus values. CI is 0.2 kg/m^3 (left) and 0.05 kg/m^3 (right).

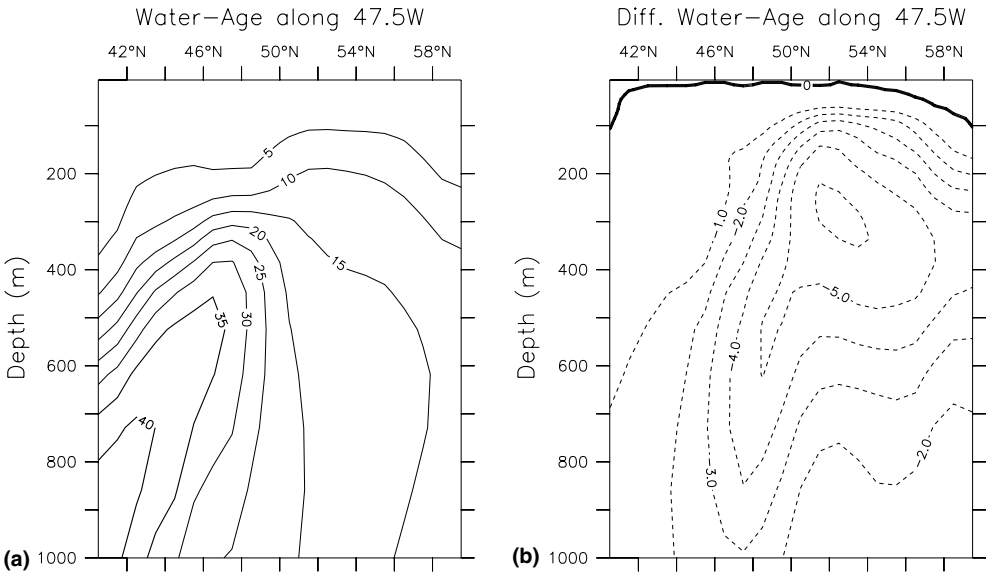

Fig. 6. Left panel is the 50 year averaged vertical distribution of ventilated water age *with* tidal mixing along 47.5° W. Right panel is the difference of ventilated water age along the same section, obtained by the subtraction the result *without* tidal mixing from *with* tidal mixing. Dashed lines in right panel are minus values. CI is 5.0 year (left) and 1.0 year (right).

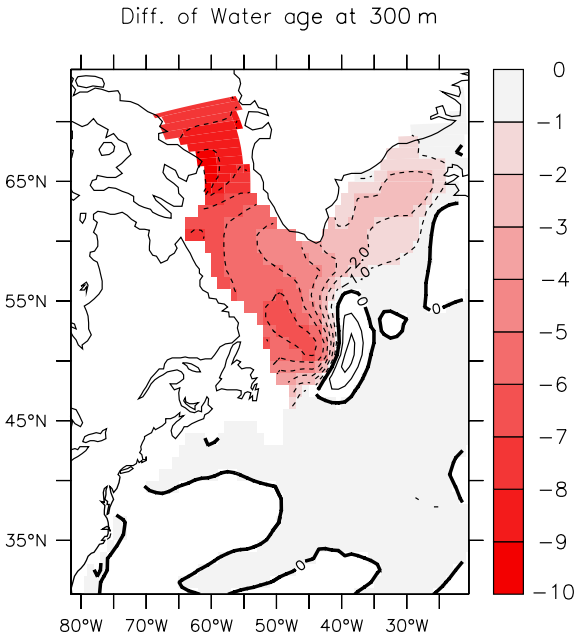

Fig. 7. Horizontal distribution of the difference of ventilated water age at 300 m depth, obtained by the subtraction the result *without* tidal mixing from *with* tidal mixing. Dashed lines are minus values. CI is 1.0 year.

comparison with the density section, the ventilation of water mass between 27.4 and 27.6σ_t occurs in the Labrador Sea between 50° N and 58° N.

The difference of water age (Fig. 6(b)) shows that the ventilated water *with* the tidal mixing is younger by up to six years than *without* tidal mixing in the Labrador Sea. The maximum difference is at 300 m depth in the Labrador Sea. Between 200 m and 600 m depth, the difference is more than three years in this region, and the impact of the tidal mixing on the meridional overturning circulation (MOC) is dominant at this depth. This clearly shows that the tidal mixing impact on the ventilation and water mass formation is concentrated in the Labrador Sea and south of Greenland (Fig. 7).

The tidal mixing effect deepens the ventilated layer in the Labrador Sea. The total volume of ventilated water within one year in the Labrador Sea (here, we took the region of 65° W–41° W, 50° N–62° N based on Fig. 7) is 0.993×10^{14} m^3 *without* tidal mixing effect and 1.085×10^{14} m^3 *with* tidal mixing effect. Net increase of ventilated water is 0.92×10^{13} m^3, and this means that the tidal mixing effect increases the amount of ventilated water by about 0.3 Sv in this region.

4. Summary and conclusion

The sensitivity of barotropic tidal mixings on oceanic conditions in the Northern Atlantic has been investigated by the GFDL coupled climate model CM2.0. The GFDL CM2.0 is based on the Flexible Model System (FMS), a model infrastructure for constructing and executing

atmospheric, oceanic and climate system models, and allows various combinations of coupled model components: atmosphere (AM2), ocean (MOM4), land (LM2) and sea ice (IM2). As the coupled model component system become more realistic, in particular river runoff and ice melting, a better physical parameterization to represent mixing due to the tide along coastal regions becomes more important. The vertical mixing driven by barotropic tide is simply parameterized from the tidal frictional turbulence with the observed tidal velocity amplitude.

The tidal mixing homogenizes vertical salinity distribution and increases the surface salinity field in the Labrador Sea by stirring the lower layer water of relatively high salinity with upper layer water. By increasing the sea surface salinity, the tidal vertical mixing increases the sea surface density (SSD) over the Labrador Sea as well as along the western coastal region of the Middle Atlantic Bight, which is in better agreement with Levitus climatology. In the Labrador Sea, the SSD from the experiment *with* tidal mixing is higher than *without* tidal mixing by 0.2 kg/m^3, and the ocean condition of denser surface water in the Labrador Sea increases the ventilation and deep water formation in the Atlantic.

The comparison of water age distribution (Fig. 6(b)) shows that the ventilated water *with* tidal mixing is younger by six years than *without* tidal mixing in the Labrador Sea, which suggests that increasing of SSD from the tidal mixing has strengthened ventilation and water mass formation processes. The tidal mixing impact on the ventilation and water mass formation is concentrated in the Labrador Sea and south of Greenland (Fig. 7). We believe these results indicate that with the increased realism in the land and ice components of coupled model requires a better representation of the coastal processes in the ocean. Since our current grid resolution requirement we chose to implement a simple parameterization of tidal mixing to overcome our model bias. Perhaps it should be said that even within this approach we noted significant impacts on SSD and ventilation and with improvement in coastal processes we may see an impacts on the variability of deep water formation and the MOC.

Acknowledgement

We thank T. Delworth, K. Dixon and R. Stouffer for their valuable discussions, A. Gnanadesikan for helpful comments and B. Arbic for the tidal velocity data. Thanks are extended to anonymous reviewers for their useful comments. We are grateful to F. Zheng and A. Langenhorst for their support.

References

Beckmann, A., Döscher, R., 1997. A method for improved representation of dense water spreading over topography in geopotential-coordinate models. J. Phys. Oceanogr. 27, 581–591.

Chapman, D.C., Beardsley, R.C., 1989. On the origin of shelf water in the Middle Atlantic Bight. J. Phys. Oceanogr. 19, 384–391.

Delworth, T.L., Broccoli, A.J., Rosati, A., Stouffer, R.J., Balaji, V., Beesley, J.A., Cooke, W.F., Dixon, K.W., Dunne, J., Dunne, K.A., Durachta, J.W., Findell, K.L., Ginoux, P., Gnanadesikan, A., Gordon, C.T., Griffies, S.M., Gudgel, R., Harrison, M.J., Held, I.M., Hemler, R.S., Horowitz, L.W., Klein, S.A., Knutson, T.R., Kushner, P.J., Langenhorst, A.R., Lee, H.-C., Lin, S.-J., Lu, J., Malyshev, S.L., Milly, P.C.D., Ramaswamy, V., Russel, J.,

Schwarzkopf, M.D., Shevliakova, E., Sirutis, J.J., Spelman, M.J., Stern, W.F., Winton, M., Wittenberg, A.T., Wyman, B., Zeng, F., Zhang, R., in press. GFDL's CM2 global coupled climate models—Part 1: Formulation and simulation characteristics. J. Climate.

Egbert, G.D., Bennett, A.F., Foreman, M.G.G., 1994. TOPEX/POSEIDON tides estimated using a global inverse model. J. Geophys. Res. 99, 24821–24852.

Egbert, G.D., Ray, R.D., 2001. Estimates of M_2 tidal energy dissipation from TOPEX/Poseidon altimeter data. J. Geophys. Res. 106, 22475–22502.

GAMDT (GFDL Atmospheric Model Development Team), submitted for publication. The new GFDL global atmosphere and land model AM2/LM2: Evaluation with prescribed SST simulations. J. Climate.

Griffies, S.M., Harrison, M.J., Pacanowski, R.C., Rosati, A., 2003. A Technical Guide to MOM4, GFDL Ocean Group Technical Report No. 5, NOAA/Geophysical Fluid Dynamics Laboratory, Available from: <http://www.gfdl.noaa.gov/~fms>.

Griffies, S.M., Gnanadesikan, A., Pacanowski, R.C., Larichev, V., Dukowicz, J.K., Smith, R.D., 1998. Isoneutral diffusion in a *z*-coordinate ocean model. J. Phys. Oceanogr. 28, 805–830.

Holloway, P., 2001. A regional model of the semidiurnal internal tide on the Australian North West shelf. J. Geophys. Res. 106, 19625–19638.

Hunke, E.C., Dukowicz, J.K., 1997. An elastic–viscous-plastic model for sea ice dynamics. J. Phys. Oceanogr. 27, 1849–1867.

James, I.D., 1977. A model of the annual cycle of temperature in the frontal region of the Celtic Sea. Estuar. Coast. Mar. Sci 5, 339–353.

Jayne, S.R., St. Laurent, L.C., 2001. Parameterizing tidal dissipation over rough topography. Geophys. Res. Let. 28, 811–814.

Large, W.G., Me Williams, J.C., Doney, S.C., 1994. Oceanic vertical mixing: A review and a model with a nonlocal boundary layer parameterization. Rev. Geophys. 32, 363–403.

Lien, R.C., Gregg, M.C., 2001. Observations of turbulence in a tidal beam and across a coastal ridge. J. Geophys. Res. 106, 4575–4591.

Lillibridge III, J.L., Hitchcock, G., Rossby, T., Lessard, E., Mork, M., Golmen, L., 1990. Entrainment and mixing of shelf/slope waters in the near-surface Gulf Stream. J. Geophys. Res. 95, 13065–13087.

Lynch, D.R., Ip, J.T.C., Naimie, C.E., Wener, F.E., 1996. Comprehensive coastal circulation model with application to the Gulf of Maine. Cont. Shelf Res. 16, 875–906.

Milly, P.C.D., Shmakin, A.B., 2002. Global modeling of land water and energy balances. Part I: The land dynamics (LaD) model. J. Hydrometeor. 3, 283–299.

Mourn, J.N., Caldwell, D.R., Nash, J.D., Gunderson, G.D., 2002. Observations of boundary mixing over the continental slope. J. Phys. Oceanogr. 32, 2113–2130.

Munk, W.H., Anderson, E.R., 1948. Notes on a theory of the thermocline. J. Marine Res. 3, 276–295.

Munk, W., Wunsch, C., 1998. Abyssal recipes II: Energetics of tidal and wind mixing. Deep-Sea Res. 45, 1997–2010.

Murray, R.J., 1996. Explicit generation of orthogonal grids for ocean models. J. Comput. Phys. 126, 251–273.

Nakamura, T., Awaji, T., 2004. Tidally induced diapycnal mixing in the Kuril Straits and its role in water transformation and transport: A three-dimensional nonhydrostatic model experiment. J. Geophys. Res. 109, C09S07. doi:10.1029/2003JC001850.

Pacanowski, R.C., Philander, S.G.H., 1981. Parameterization of vertical mixing in numerical models of tropical oceans. J. Phys. Oceanogr. 11, 1443–1451.

Schiller, A., 2004. Effects of explicit tidal forcing in an OGCM on the water-mass structure and circulation in the Indonesian throughflow region. Ocean Modell. 6, 31–49.

Semtner, A.J., 1976. A model for the thermodynamic growth of sea ice in numerical investigations of climate. J. Phys. Oceanogr. 6, 27–37.

Simmons, H.L., Jane, S.R., St. Laurent, L.C., Weaver, A.J., 2004. Tidally driven mixing in a numerical model of the ocean general circulation. Ocean Modell. 6, 245–263.

Simpson, J.H., Hunter, J.R., 1974. Fronts in the Irish Sea. Nature 250, 404–406.

St. Laurent, L.C., Simmons, H.L., Janye, S.R., 2002. Estimating tidally driven mixing in the deep ocean. Geophys. Res. Lett. 29, 2106. doi:10.1029/2002GL015633.

Werner, S.R., Beardsley, R.C., Lentz, S.T., Hebert, D.L., Oakey, N.S., 2003. Observations and modeling of the tidal bottom boundary layer on the southern flank of Georges Bank. J. Geophys. Res. 108 (C11), 8005. doi:10.1029/2001JC001271.

Winton, M., 2000. A reformulated three-layer sea ice model. J. Atmos. Ocean. Technol. 17, 525–531.

Winton, M., 2003. On the climate impact of ocean circulation. J. Climate 16, 2875–2889.